Prediction of Ignition Transients in Solid-Propellant Rocket Motors

RICHARD H. SFORZINI*
Auburn University, Auburn, Ala.
AND
HUGH L. FELLOWS JR.†
Martin Marietta Corporation, Orlando, Fla.

Nomenclature

A_b = surface area of propellant burning
A_p = chamber port cross-sectional area
A^* = throat cross-sectional area
a,b = constants in $c^* \simeq a + bP_c$
c^* = characteristic velocity
C = burning rate coefficient in $r = CP^n$
$J \equiv A^*/A_p$
$\dot{m}_d$ = mass discharge rate through rocket motor nozzle
$\dot{m}_g$ = mass rate of gas generation inside the chamber
$\dot{m}_i$ = rate of mass flow from igniter into the chamber
$\dot{m}_{V_c}$ = rate of gas accumulation inside the chamber
n = burning rate exponent in $r = CP^n$
P = static pressure; $\bar{P} \equiv (P_1 + P_2)/2$
P_c = chamber pressure, or nozzle-end stagnation pressure
r = burning rate
R = gas constant of chamber gases
t = time, measured from firing switch closure
T_c = absolute flame temperature of chamber gases
V_c = free volume of the rocket chamber
v_f = flame-spreading speed
γ = ratio of specific heats of combustion gases
Γ = a function of γ defined by Eq. (4)
ρ_c = density of chamber gases
ρ_p = density of solid propellant

Subscripts

i = igniter
1,2 = head end and aft-end stations (Fig. 1)

Introduction

QUANTITATIVE knowledge of the pressure overshoot during ignition ($P_{c\max}$) and the maximum pressure rise rate $(dP_c/dt)_{\max}$, both of which tend to be augmented in modern, high-volumetric-loading-density solid-propellant rocket motors (SRM's), is important to the preliminary designer in determining structural capacity of inert components and the visco-elastic propellant.

Propellant response to ignition initiation processes is known to depend not only on a number of environmental conditions but also on the propellant and the nature of the initiating stimulus.[1] De Soto and Friedman have developed a mathematical model of ignition wherein the flame-spreading speed v_f is evaluated in terms of the heat-transfer from the gases in the chamber, which is assumed to take place at constant temperature.[2] They assumed a gasless igniter and initially choked flow. Their heat-transfer analysis is quite complete, but uncertainty exists on the proper expressions for heat-transfer coefficients to be used, and no comparison of theory with experiment is given.

Received December 22, 1969; revision received February 17, 1970. This research was performed at Auburn University in conjunction with the Master of Science in Aerospace Engineering program of H. L. Fellows Jr. The authors wish to acknowledge the helpful assistance of G. E. Webb, Chief of the Igniter Section, Huntsville Division, Thiokol Chemical Corporation, who supplied experimental results and other data for the numerical examples solved in this paper.

* Professor, Aerospace Engineering. Member AIAA.
† Engineer, Propulsion Section, Engineering Department.

The present analysis for $P_c(t)$ accounts for changes in flame temperature with pressure, secondary mass addition by the igniter and the flame-spreading phenomenon, with v_f treated as a phenomenological constant whose value is deduced by comparison of theoretical and experimental results. The following assumptions are made (a few more are made later):

1) V_c and A_b are constant during the ignition transient.
2) The combustion gases obey the perfect gas law.
3) The area ratio J $(= A^*/A_p)$ is sufficiently small that P_c may be taken as a good approximation to the pressure governing the burning rate r throughout the length of the rocket motor: $r = CP_c^n$
4) The effect of velocity on r (erosive burning) is negligible.
5) Gas flow is one-dimensional.
6) The nozzle undergoes choking immediately and is choked throughout the ignition phase, and mass is accumulated only in the chamber (ahead of the nozzle).
7) The characteristic velocity c^* of the chamber gases is linearly related to chamber pressure: $c^* \simeq a + bP_c$
8) The flame-spreading speed v_f during ignition is constant.

Assumption 1 is justifiable for the ordinary burning rates ($\bar{r} \lesssim 0.5$ in./sec) and moderate ignition transient times ($\sim$60 msec) considered here. Assumption 2 holds reasonably well for gases above their critical temperatures and below their critical pressures. The significance of assumption 3 is discussed later. Assumption 4 is valid when J is small, resulting in low velocities in the grain port; for higher velocities, it is questionable. In internal ballistics studies of SRM's, assumption 5 has been customary and satisfactory.[2] Per assumption 6, the analysis will produce only that portion of the pressure time trace occurring after the nozzle is choked (the portion prior to choking is usually very small in comparison), and the transit time through the nozzle is considered negligible with respect to the time required to produce a substantial pressure change in the chamber.[3] The validity of assumption 7 may be partially judged from typical thermochemical data for $c^*(P_c)$ presented later in the paper (except at very low pressure, $c^*(P_c)$ is roughly linear); the assumption also implies infinite chemical reaction rates (shifting chemical equilibrium).

Although assumption 8 may be the weakest of the lot (indeed, since ignition is fundamentally dependent on heat transfer to the grain surface, it is to be expected that the changing P_c during ignition would have a strong influence on v_f), let us assume that an average (constant) value is adequate to define the essential influence of v_f on P_c during ignition.

Derivation of the Governing Equations

A mass balance based on Fig. 1 is written:

$$\dot{m}_i + \dot{m}_g = \dot{m}_d + \dot{m}_{V_c}; \quad \dot{m}_{V_c} = d(\rho_c V_c)/dt \qquad (1)$$

For steady flow through a choked nozzle (assumption 6), $\dot{m}_d = P_c A^*/c^*$. Similarly, for a gaseous type igniter, which is frequently a scaled-down SRM, we can use $\dot{m}_i = (P_c A^*/c^*)_i$ for that portion of the ignition phase when the igniter is delivering choked flow. The chamber mass rate

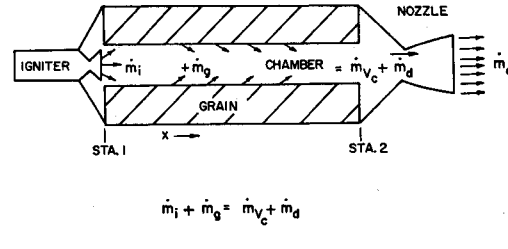

Fig. 1 Schematic of SRM and mass balance model.

Table 1 Characteristics of the three example motors

Parameter	SRM 1	SRM 2	SRM 3
Grain configuration	Slotted tube	5-point star	5-point star
r @ 1,000 psia, in./sec	0.735	0.711	0.594
c^* @ 1,000 psia, ft/sec	5,190	5,180	5,020
γ	1.15	1.16	1.19
$J_2 = A^*/A_{p2}$	0.401	0.578	0.492
Initial V_c, in.^{3}	18,760	7,860	1,600
Igniter A^*, in.^{2}	1.809	0.819	0.403

of gas generation is $\dot{m}_g = \rho_p A_b \bar{r}$, where $\bar{r}$ is the average regression rate of the ignited surface. Since we have assumed that chamber geometry remains unchanged during the ignition transient, A_b is a function only of the flame spreading for a particular SRM.

By assumption 3, we use P_c, the stagnation pressure at the aft end of the grain as the pressure governing the burning rate throughout the length of the grain. Let us examine this assumption. For steady SRM chamber flow[3]

$$P_1/P_c \simeq 1 + \Gamma^2 J^2/2 \tag{2}$$

and

$$P_2/P_c \simeq 1 - \Gamma^2 J^2/2 \tag{3}$$

where

$$\Gamma \equiv \gamma^{1/2}[2/(\gamma + 1)]^{(\gamma+1)/2(\gamma-1)} \tag{4}$$

Approximations Eqs. (2) and (3), obtained from a truncated Taylor series expansion of the steady-state continuity equation for chamber flow in terms of P_1/P_c,[3] are accurate when $P_1/P_c \to 1$; e.g., Eq. (2) yields 1.075 for P_1/P_c, compared to an "exact" value of 1.078 when $\gamma = 1.24$ and $J = 0.6$. When Eqs. (2) and (3) are added, they yield $P_c \simeq \bar{P} \equiv (P_1 + P_2)/2$; thus it seems reasonable to use P_c as the pressure governing.

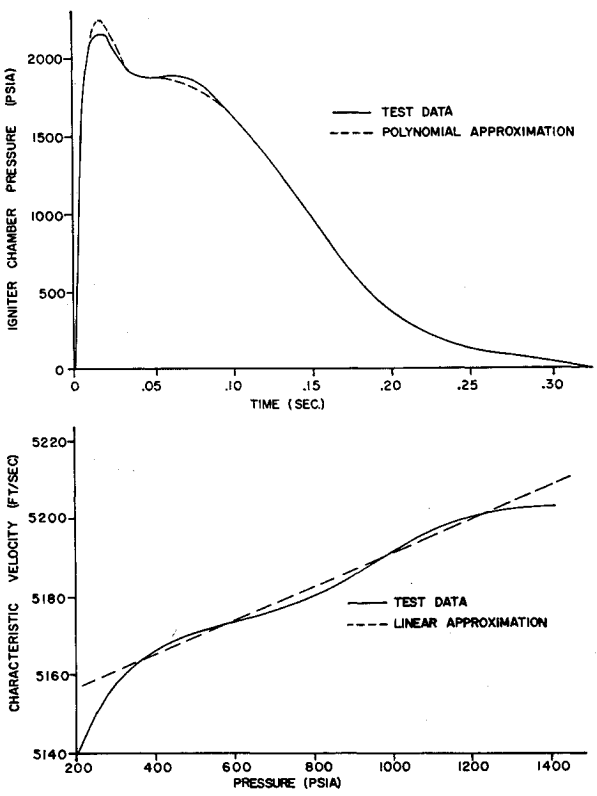

Fig. 2 Igniter chamber pressure and main motor characteristic velocity for example SRM number 1.

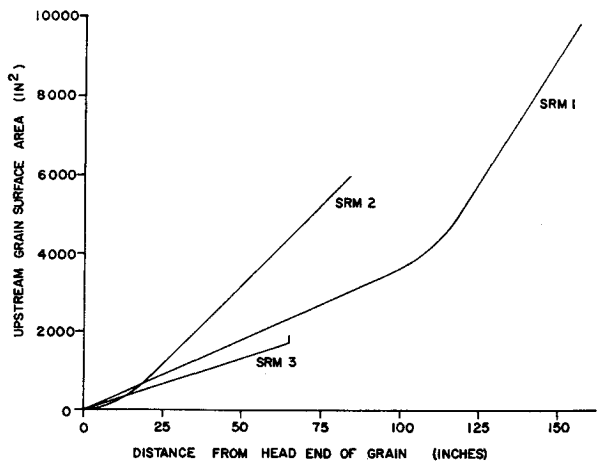

Fig. 3 Burning surface area vs position of the flame front for example SRM's.

Now, upon expanding the right-hand side of Eq. (1) and noting that, by assumption 1, $dV_c/dt = 0$, we obtain

$$\dot{m}_i + \rho_p A_b C P_c^n = P_c A^*/c^* + V_c d\rho_c/dt \tag{5}$$

Using assumption 2, we obtain $d\rho_c/dt$ in the form

$$d\rho_c/dt = (1/RT_c)dP_c/dt - (P_c/RT_c^2)dT_c/dt \tag{6}$$

We can express c^* as[3]

$$c^* = (RT_c)^{1/2}/\Gamma \simeq a + bP_c \tag{7}$$

where the approximation is assumption 7. Differentiation of Eq. (7) with respect to time yields

$$dT_c/dt = [2b\Gamma^2(a + bP_c)/R]dP_c/dt \tag{8}$$

Substituting Eqs. (6–8) into Eq. (5) and solving for dP_c/dt, we obtain

$$dP_c/dt = [\dot{m}_i + \rho_p A_b C P_c^n - A^* P_c/(a + bP_c)] \times \Gamma^2(a + bP_c)^3/V_c(a - bP_c) \tag{9}$$

Results and Discussion

Equation (9) is nonlinear in P_c, with time-dependent coefficients $\dot{m}_i$ and $C\rho_p A_b$ in addition to the coefficients a and b of the linear c^* equation. A numerical solution was developed for integration of this equation based on a Runge-Kutta solution of the fourth order,[4] and a computer program was prepared to perform the calculations for three case-bonded, internal-burning SRM's (Table 1). The propellants were of the composite type with ammonium perchlorate oxidizer and aluminum additives.

Using the methods of least squares, quintic relations were fitted in two sections to the traces of $P_c(t)$ for each igniter. The forms of the $P_{ci}(t)$ for the igniter and $c^*(P_c)$ for the main motors were similar for each motor investigated (Fig. 2 shows them for SRM 1). The igniter curves for each motor were based upon data from test firing of companion igniter motors manufactured to the same specifications. Performance will differ somewhat for the two cases. As main motor pressure rises and igniter pressure falls, the igniter nozzle will become unchoked earlier in the main motor than in the test of the companion igniter motor. However, the unchoking occurs when the amount of mass contributed by the igniter is small in comparison to that contributed by the main motor.

Figure 3 shows A_b vs position of the flame front for the three motors. The variation of $\dot{m}_g$ was based upon a plot of A_b vs the length burning, the latter being readily computed from v_f (assumed constant). For the first example, various v_f's were assumed and $P_c(t)$ was calculated and compared to

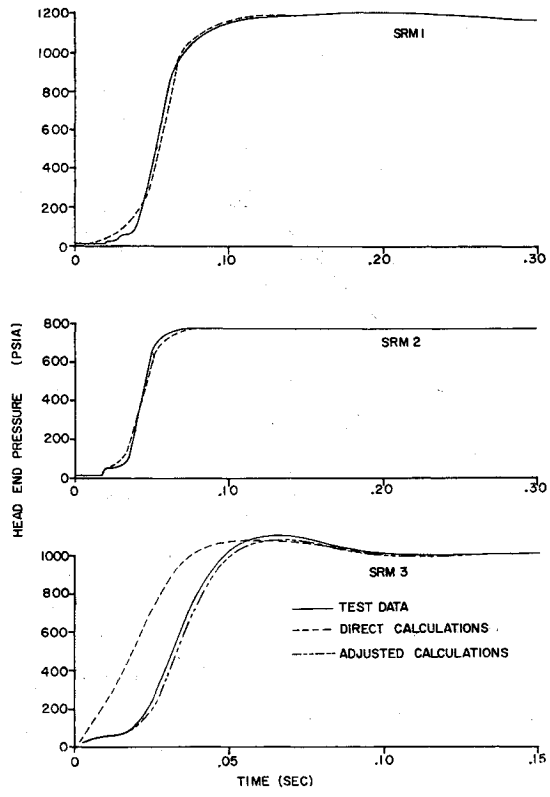

Fig. 4 Comparison of calculated chamber pressure with test results.

experimental results: $v_f = 3650$ in./sec yielded best agreement and was chosen for use in the first numerical example, and then applied to the other two numerical examples. The resulting comparisons are shown in Fig. 4. Two calculations are indicated for SRM3. In the first calculation the initial pressure rise occurred too soon. To investigate this, a pressure-time trace was calculated in which only the igniter furnished pressurization to the SRM. This trace was identical to the test trace for the first 16 msec. An adjusted trace was then computed in which the grain was first ignited after 16 msec. The "adjusted" curve in Fig. 4 agrees well with the test trace.

The transient ignition problem as studied herein can be divided into two phases: flame-spreading and chamber-filling. The flame-spreading portion of the $P_c(t)$ trace begins with zero slope and arcs upward to a position where the slope is approximately a maximum. The chamber-filling interval is the interval between complete ignition of the propellant surface and the time at which essentially steady chamber conditions are reached; it occupies the larger part of the ignition transient time. It is notable that $(dP_c/dt)_{\max}$ and $P_{c\max}$, which are the most important factors to be determined, are predicted quite well for all three motors, apparently because the chamber-filling phase is more important than the flame-spreading phase. Also, even for SRM 3, the analysis yields at least a first estimate of the transients during the initial phase.

Refinements to this analysis are possible. The variation of gaseous properties throughout the grain length could be more accurately determined by dividing the grain into short segments and solving the momentum, energy, and state equations in turn for each segment by an iterative technique until an over-all mass balance is achieved. An erosive burning law could also be included.

References

[1] Price, E. W. et al., "Theory of Ignition of Solid Propellants," *AIAA Journal*, Vol. 4, No. 7, July 1966, pp. 1153–1181.

[2] de Sota, S. and Friedman, H. A., "Flame Spreading and Ignition Transients in Solid Grain Propellants," *AIAA Journal*, Vol. 3, No. 3, March 1965, pp. 405–412.

[3] Barrère, M. et al., *Rocket Propulsion*, 1st ed., Elsevier, Amsterdam, 1960, pp. 237–243 and pp. 255–256.

[4] Ralston, A., *A First Course in Numerical Analysis*, 1st ed., McGraw-Hill, New York, 1965, p. 200.

Angle of Attack and Lateral Rate for Nearly Circular Re-Entry Motion

Mark M. Lotkin*
General Electric Company, Philadelphia, Pa.

Nomenclature

A = reference area of vehicle
a = scale height
C_D = drag coefficient
$C_{M\alpha}$ = pitching moment coefficient slope
d = reference diameter of vehicle
H = $h_0 - h$
h = geometric altitude; $h_0 = h(t_0)$ at re-entry
I_x, I_y = roll and pitch moments of inertia
k = $AC_D/am \sin\gamma_0$ = "drag" parameter
m = mass of vehicle
q_∞ = $\rho V^2/2$ = dynamic pressure
s = total lateral angular rate
t = time
V = relative velocity of vehicle
γ = flight path angle
δ = total angle of attack
ρ = density of air
ω = body-fixed frequency of vehicle

Subscripts

$(\ )_0$ = at arbitrary altitude h_0; see Eqs. (7)
$(\ )_s$ = at sea level, $h_s = 0$

Introduction

In a previous article[1] there was derived a set of ordinary first-order differential equations for the total angle-of-attack δ and the relative roll angle μ in terms of the vehicle's roll, pitch, and yaw rates. These equations apply to the exosphere as well as the atmosphere, and for angles of arbitrary magnitude. In this Note these basic equations are applied to the case of nearly circular angle-of-attack motion during re-entry, for small angles of attack. The use of well-known expressions for the frequencies of the lateral rates permits an integration of the differential equation for a mean value of δ, leading to an expression of a mean total lateral rate as well. The general expressions thus obtained are applied to cases that are typical of the high-altitude trajectory of advanced re-entry vehicles, leading to approximations of potential utility in simulations of pertinent trajectories. Finally, a typical example is given.

Differential Equations

In Ref. 1 it was shown that δ and μ satisfy

$$\dot{\delta} = s \sin(\mu - \epsilon) \tag{1}$$

$$\dot{\mu} = -p + (s/\tan\delta) \cos(\mu - \epsilon) \tag{2}$$

with

$$s^2 = q^2 + r^2 \qquad \tan\epsilon = r/q \tag{3}$$

Received December 23, 1969.

* Consultant, Re-entry and Environmental Systems Division.